Check for updates

Parolari Anthony (Orcid ID: 0000-0002-1046-6790)

Precipitation variability can bias estimates of ecological controls on ecosystem productivity response to precipitation change

Anthony J. Parolari[1,*] and Athanasios Paschalis[2]

[1]Department of Civil, Construction, and Environmental Engineering, Marquette University, Milwaukee, WI

[2]Department of Civil and Environmental Engineering, Imperial College London, London, UK

*Corresponding author: anthony.parolari@marquette.edu, 414-288-3508

Abstract

Annual vegetation aboveground net primary productivity (ANPP) exhibits a nonlinear dependence on annual precipitation. A common pattern of nonlinearity, called asymmetry, arises when productivity responses in wet years are larger than declines in dry years. To-date, ANPP asymmetry has been attributed primarily to vegetation water stress, an internal ecosystem response to precipitation and soil water availability. However, when quantified via the asymmetry index (AI) estimated from productivity measurements, the asymmetry can be a sampling artifact that arises from a positively skewed annual precipitation distribution. In this paper, we aimed to separate the sampling effect (from external precipitation variability) from the nonlinear response of the system (the internal ecosystem dynamics). We constructed a probabilistic model that integrates the precipitation distribution with the precipitation-productivity response curve (PPT-ANPP curve), derived using empirical formulae and a process-based soil water balance model. The model was used to derive the probability density function of AI and to attribute its shape to the PPT distribution and the PPT-ANPP response curve. The models were compared to data from 47 grasslands. Results demonstrated that positively skewed precipitation produces a positive AI as a statistical artifact. The nonlinear ecosystem PPT-ANPP dependance can further enhance or dampen this statistical artifact. In all sites, the precipitation skew highly affected the probability of correctly identifying asymmetry

This article has been accepted for publication and undergone full peer review but has not been through the copyediting, typesetting, pagination and proofreading process which may lead to differences between this version and the Version of Record. Please cite this article as doi: 10.1002/eco.2384

This article is protected by copyright. All rights reserved.

Accepted Article

using AI. Observed negative asymmetry arises from a larger soil water holding capacity, and positive asymmetry from plant water stress. More robust statistical indicators of nonlinear ecological responses to climate variability are needed to improve ecosystem forecasts.

Keywords: asymmetry index, climate extremes, drought, precipitation, productivity, soil water balance, stochastic modeling, ecological statistics

1. Introduction

The response of terrestrial ecosystem productivity to precipitation is critical to the global carbon cycle and atmospheric CO_2 dynamics (Ahlström et al., 2015; Humphrey et al., 2018; Poulter et al., 2014). Precipitation has changed in the twentieth century in complex ways, including changes in annual precipitation amounts with increases in both wet and dry precipitation extremes at daily to interannual scales (Easterling, 2000; Fischer & Knutti, 2015; Kunkel et al., 2013; Lenderink & Van Meijgaard, 2008; Molnar et al., 2015; Moustakis et al., 2020, 2021; Pendergrass & Knutti, 2018; Peterson et al., 2013). At the same time, photosynthesis and above-ground net primary productivity at the annual scale (ANPP) have been shown to respond to both total annual precipitation and the timing and intensity of individual rain events throughout the year (Heisler-White et al., 2009; Knapp et al., 2002, 2008; Knapp & Smith, 2001). Therefore, future precipitation regimes anticipated with further climate change are hypothesized to impact primary production and the strength of the land carbon sink.

Grasslands in particular, that grossly support global food production (O'Mara, 2012), and play a dominant role in the interannual variability of the land carbon sink (Ahlström et al., 2015; Piao et al., 2020), are vulnerable to increased periods of drought (e.g. (Konings et al., 2017)). Considering that grasslands to a large extent are located in regions where dry conditions are expected to increase (Greve & Seneviratne, 2015; Koutroulis, 2019), it is crucial to understand their responses to water availability, and precipitation in particular. Grassland ANPP response to annual precipitation, derived from decades of ecosystem productivity experiments, was recently summarized in the 'double asymmetry' conceptual model (Knapp et al., 2017). The double asymmetry model proposes two primary ANPP responses to precipitation. During years with non-extreme rainfall totals (i.e. with deviations within approximately 2 standard deviations of the observed long-term mean), ANPP exhibits a larger positive response relative to its mean to precipitation increases than negative response to precipitation decreases. This

This article is protected by copyright. All rights reserved.

response type is called "positive asymmetry." On the other hand, during extreme dry or wet years, ANPP exhibits the opposite behavior – that is, negative asymmetry.

The occurrence of positive or negative asymmetry is partly controlled by the ecosystem response to precipitation, encapsulated at the annual scale in the precipitation-productivity curve (or the PPT-ANPP curve). The PPT-ANPP curve is a mathematical function that relates annual precipitation totals to annual ANPP at a given site. Both linear and non-linear PPT-ANPP curves have been fit to experimental data (Hsu et al., 2012) and simulated using ecohydrological models that resolve the coupled water and carbon cycles (Istanbulluoglu et al., 2012; Parolari et al., 2015; Wu et al., 2018). The degree of non-linearity in the PPT-ANPP curve controls whether the productivity response exhibits positive or negative asymmetry and, therefore, how productivity will respond to changes in precipitation extremes (Ahlström et al., 2015; Haverd et al., 2017; Hsu et al., 2012; Humphrey et al., 2018; Poulter et al., 2014). Convex (Concave) PPT-ANPP curves lead to positive (negative) asymmetry and an increased (decreased) mean ANPP with increased precipitation variance (Hsu et al., 2012). Therefore, the non-linearity of the ANPP response to precipitation is critical to quantifying how the carbon cycle will respond to changes in the distribution of annual precipitation. The non-linearity of ecosystem carbon cycle responses to precipitation changes are particularly important because climate change projections suggest an increase in precipitation extremes.

Asymmetry has been commonly quantified using the asymmetry index (AI), defined as the difference between positive and negative deviations from the long term mean ANPP,

$$AI = \left(\frac{a_{max}-\mu_a}{\mu_a}\right) - \left(\frac{\mu_a-a_{min}}{\mu_a}\right) \quad (1)$$

where a_{max} and a_{min} are the maximum and minimum of an observed ANPP time-series, respectively, and μ_a is the observed mean ANPP. When the positive ANPP deviations from the mean are smaller than the negative deviations, AI is negative (and vice versa). AI is estimated directly from ANPP observations sampled annually over multiple years and it inherently combines the ecosystem response to precipitation (i.e., PPT-ANPP curve) as well as the statistics of annual precipitation. Annual precipitation distributions are often positively skewed (Fatichi et al., 2012) and samples of positively skewed variables exhibit positive asymmetry. Therefore, positive skew of the annual precipitation distribution may introduce

This article is protected by copyright. All rights reserved.

bias when estimating asymmetry from annual ANPP observations alone, leading to incorrect conclusions about the non-linearity of the ecosystem response to precipitation (see Figure 1 and caption for examples). The influence of the annual precipitation distribution on the statistics of AI is unknown, but is critical to the interpretation of asymmetry calculated from ANPP data.

In this paper, we analyze the statistics of the asymmetry index using probabilistic and process-based ecohydrological models. These models are used to quantify the relative contributions of the inherent nonlinear ecosystem PPT-ANPP behavior and the distribution of annual PPT, and identify the underlying physical mechanisms. Applying the models to 47 grasslands worldwide, we identify for the first time the importance of sampling artifacts derived from inter-annual precipitation variability on assessment of asymmetric ecosystem responses to changes in precipitation.

2. Materials and Methods

2.1 Statistics of multi-year ANPP experiments

The asymmetry index, AI, can be interpreted as a random variable with a corresponding probability density function (PDF), $f_{AI}(AI)$. The distribution $f_{AI}(AI)$ quantifies the probability of observing either positive or negative asymmetry during a multi-year ANPP experiment with N observations and can be considered the sampling distribution of AI. Through equation (1), $f_{AI}(AI)$ depends on the PDF of the observed annual ANPP, $f_A(a)$, and the corresponding joint PDF of the maximum and minimum values, $f_{A_{max},A_{min}}(a_{max}, a_{min})$. Expressions for $f_A(a)$ and $f_{A_{max},A_{min}}(a_{max}, a_{min})$ are derived in the Supplementary Material, sections S1 and S2, respectively.

The distribution $f_{AI}(AI)$ can be derived using two assumptions. First, assume precipitation in any year is an independent sample from an underlying distribution, $f_{P_a}(p_a)$, where p_a is the annual precipitation amount. Second, assume ANPP is a deterministic and monotonically increasing function of p_a, i.e., $a = g(p_a)$, where g is the PPT-ANPP curve. Finally, note that equation (1) can be rewritten as $AI = \frac{S}{\mu_a} - 2$, where $S = a_{max} + a_{min}$ is the sum of the minimum and maximum observed ANPP values. The distribution of S is, by definition,

This article is protected by copyright. All rights reserved.

$$f_S(S) = \int_{-\infty}^{\infty} f_{A_{max},A_{min}}(a, S-a)da. \quad (2)$$

Because AI is a linear function of S, the PDF of AI can be written as,

$$f_{AI}(AI) = \mu_a f_S[\mu_a(AI+2)]. \quad (3)$$

where $\mu_a = \int_0^{\infty} a f_A(a)da$ is the expected value of annual ANPP. Equation (3) is valid only for independent and identically distributed annual PPT and ANPP and, therefore, cannot be generalized to cases where significant trends or autocorrelations are present in either signal.

Equation (3) describes the sampling distribution for the sign and magnitude of AI, given an annual precipitation distribution, a PPT-ANPP response curve, and the length of the experiment. Therefore, to complete equation (3), definitions of $f_{P_a}(p_a)$ and $g(p_a)$ are needed. In this study, the precipitation distribution, $f_{P_a}(p_a)$ was assumed to be either normal or lognormal with a specified mean and variance that are constant in time. The assumed PPT-ANPP models, $g(p_a)$ are described below.

2.2 Precipitation-productivity response models

Four models were used to define the PPT-ANPP curve. Three purely statistical models at the annual scale and one mechanistic ecohydrological model operating at the daily scale. The statistical models are: linear, nonlinear concave, and nonlinear convex; and the ecohydrological model is a minimalist physically-based soil water balance that relates soil water availability to plant productivity (Porporato et al., 2004). The linear and nonlinear models were fit to experimental data using least squares regression (Hsu et al. 2012). The statistical models were used to quantify the relative contributions of the precipitation distribution and the PPT-ANPP curve to AI, while the ecohydrological model was used to identify the ecohydrological mechanisms that contribute to the PPT-ANPP curve shape and its effect on AI.

Linear model. The assumed linear PPT-ANPP curve is,

$$a = wp_a + a_0 \quad (4)$$

This article is protected by copyright. All rights reserved.

where a (g DM m^{-2}) is the annual ANPP, w (g DM m^{-2} mm^{-1}) is a precipitation-use efficiency, p_a (mm) is the annual precipitation, a_0 (g DM m^{-2} yr^{-1}) is the zero precipitation intercept, and DM indicates dry mass (Hsu et al., 2012). The intercept a_0 is valid within the observed range of precipitation only.

Nonlinear concave model. The assumed non-linear concave PPT-ANPP curve is,

$$a = a_m - bp_a^{-1} \tag{5}$$

where a_m (g DM m^{-2} yr^{-1}) is the maximum ANPP and b (g DM m^{-2} mm yr^{-1}) is a parameter that controls the sensitivity of a to p_a (Hsu et al., 2012). The curvature of equation (5) is always negative, i.e., $g''(p_a) = -2bp_a^{-3} < 0$.

Nonlinear convex model. A non-linear convex PPT-ANPP curve is proposed to capture non-linear behavior not modeled by equations (4) and (5) above, but that has been identified in ANPP experiments (e.g., Parolari et al., 2015). This model is,

$$a = \omega p_a^{\beta} \tag{6}$$

where ω (g DM m^{-2} mm$^{-\beta}$) is a precipitation use efficiency and β is an exponent that controls the non-linearity of the ANPP response to PPT. The curvature of equation (6) is positive for $\beta > 1$, i.e., $g''(p_a) = \beta(\beta - 1)\omega p_a^{\beta-2}$.

Daily-scale piece-wise linear productivity with explicit soil water balance model. For climates where the growing season occurs during the wet season, a PPT-ANPP curve with a mechanistic basis can be derived from the approach described by Porporato et al. (2004). The model assumptions are as follows: Precipitation is assumed to be a marked Poisson arrival stochastic process with mean rate, λ (d^{-1}), and exponentially-distributed daily depths with mean depth, α (mm). The homogeneous marked Poisson process model of daily-scale precipitation is consistent with the long-term mean annual precipitation, but does not generate a skewed distribution of annual precipitation. Precipitation is partitioned into a rapid leakage/runoff process and slower evapotranspiration. Because the leakage/runoff process is rapid and highly non-linear, it is assumed to occur instantaneously at the daily-scale above a threshold soil

This article is protected by copyright. All rights reserved.

moisture value, s_1. Evapotranspiration (ET) is assumed to vary as a linear function of soil moisture between 0 at the wilting point, s_w, and a potential, ET_{max} (mm d^{-1}), at saturation (s_1). Net carbon assimilation rate, A, is assumed to achieve its maximum value, A_{max} (g DM m^{-2} d^{-1}) above a soil moisture threshold, s^*, and decreases linearly below s^* to 0 at a lower threshold, s_{cr} (Daly et al., 2004; Feng et al., 2012). For parsimony, the seasonal pattern of leaf area index that would affect A_{max} is neglected.

For $s_{cr} = s_w$, the PPT-ANPP curve from this model is,

$$a = f_a A_{max} T_{seas} \left\{ \frac{1}{x^* \gamma} \cdot \left[\frac{\Gamma\left(\frac{\lambda}{\eta}+1\right) - \Gamma\left(\frac{\lambda}{\eta}+1, \gamma x^*\right)}{\Gamma\left(\frac{\lambda}{\eta}\right) - \Gamma\left(\frac{\lambda}{\eta}, \gamma\right)} \right] + \left[\frac{\Gamma\left(\frac{\lambda}{\eta}, \gamma x^*\right) - \Gamma\left(\frac{\lambda}{\eta}, \gamma\right)}{\Gamma\left(\frac{\lambda}{\eta}\right) - \Gamma\left(\frac{\lambda}{\eta}, \gamma\right)} \right] \right\} \quad (7)$$

where: f_a, is the fraction of net assimilation allocated above-ground; A_{max} (g DM m^{-2} d^{-1}), the maximum daily net assimilation rate; T_{seas} (d), the growing season length; x^*, the relative soil moisture, $(s^* - s_w)/(s_1 - s_w)$; $\gamma = nz_r(s_1 - s_w)/\alpha$, the ratio of soil water holding capacity to mean rainfall depth α (where n and z_r (mm) are the porosity and root zone depth, respectively); and $\eta = ET_{max}/nz_r(s_1 - s_w)$ is the ratio of the maximum ET rate to the soil water holding capacity. $\Gamma(a, b) = \int_b^\infty x^{a-1} e^{-x} dx$ is the upper incomplete gamma function (Abramowitz & Stegun, 1972). Note that the annual precipitation is $p_a = \alpha \lambda T_{seas}$. The parameters α and λ contribute separately to the nonlinearity of the PPT-ANPP curve, as shown in the second term on the right-hand side of equation (7). T_{seas} scales the maximum daily aboveground productivity, $f_a A_{max}$, to the annual scale, and is considered as a constant in the present analysis. Equation (7) and a more general version of this model for $s_{cr} > s_w$ are derived in the Supplementary Material, Section S3. The model exhibits positive curvature for low values of precipitation and negative curvature for high values of precipitation only when $s_{cr} > s_w$.

The goal of equation (7) is solely to provide a mechanistic dependence of ANPP on annual P (i.e., the PPT-ANPP curve). The underlying mechanistic assumptions include the statistics of individual storm frequency and depth, the soil water holding capacity, and the daily-scale evapotranspiration and productivity response to soil moisture. For further analysis of the effect of annual precipitation skewness on AI, we use equation (7) in a similar fashion to the linear and nonlinear empirical models (equations (4)-(6)).

This article is protected by copyright. All rights reserved.

2.3 Case study data

As a detailed case study, PPT and ANPP data from Konza Prairie was used (Knapp et al., 2017; Knapp & Smith, 2001). Konza Prairie is a perennial tallgrass prairie located in northeastern Kansas. The climate is temperate, mid-continental with mean annual rainfall of 847 mm and standard deviation 170 mm, calculated for the period 1991-2013. The distribution of annual rainfall is well described by a lognormal distribution. The soils are deep silty clay loam and the site is burned annually. Site details were taken from (Fay et al., 2000). ANPP estimates were derived using aboveground biomass harvest in representative plots under ambient precipitation (23 years) as well as irrigation (8 years) and drought treatments (2 years) (Hoover et al., 2014; Knapp et al., 2017; Wilcox et al., 2016). The linear (equation 4) and nonlinear concave (equation 5) statistical models were previously fit to the Konza Prairie data (Hsu et al., 2012; Knapp et al., 2017). The minimalist model (equation 7) was applied to the Konza Prairie data with parameters estimated from previous studies, reported in Table 1 in the results.

To further support our analysis we used the data reported in Hsu et al. (2012) to estimate the AI distribution, $f_{AI}(AI)$ (equation 3), and the relative contributions of the precipitation distribution and the PPT-ANPP curve to the shape of $f_{AI}(AI)$. Hsu et al. (2012) compiled and analyzed 58 long-term ANPP datasets, 46 of which correspond to grasslands and were used here. For each site, this dataset includes the number of years, annual precipitation, and ANPP values. Growing season precipitation was used instead of annual precipitation in cases where it was a better predictor of ANPP, which is also accounted for in equation (7) by rescaling according to the growing season length. The dataset also includes the best fit precipitation distribution (normal or lognormal) and linear and non-linear PPT-ANPP response curves (equations 4 and 5) fit to the data. The Akaike information criterion (AIC) weight was calculated for the linear model to identify the best fit PPT-ANPP curve.

2.4 Statistical analysis

For each of the 46 grasslands, we first calculated the distribution of AI, $f_{AI}(AI)$, using the best fit precipitation distribution and the PPT-ANPP curve with the highest AIC weight. The total asymmetry at each site was defined as the mode of this distribution, i.e., the most likely value to be observed from a sample of ANPP values. Next, we separated the total asymmetry into an external asymmetry, due to the precipitation distribution, and an internal asymmetry, due to the PPT-ANPP curve. The external asymmetry was defined as the mode of the AI distribution

This article is protected by copyright. All rights reserved.

calculated for the observed precipitation distribution and the reported linear model fit. The internal asymmetry was defined as the mode of the AI distribution calculated for a normal precipitation distribution with the observed mean and standard deviation and the PPT-ANPP curve with the highest AIC weight. Therefore, the external asymmetry represents the skew generated by the precipitation distribution and the internal asymmetry represents the skew generated by the PPT-ANPP curve.

3. Results

3.1 The asymmetry index distribution

First, in this section, we study the sensitivity of the modeled asymmetry index distribution to the model inputs. The skewness of $f_{AI}(AI)$ and its bias toward positive or negative values depends on several factors related to the model inputs (Figure 2). When the annual precipitation distribution is normal and the PPT-ANPP curve is linear, $f_{AI}(AI)$ is symmetric about $AI = 0$ (Figure 2a). That is, there is an equal probability of observing positive or negative asymmetry in a field experiment, regardless of the parameters for either $f_{p_a}(p_a)$ or $g(p_a)$. The symmetry of $f_{AI}(AI)$ for this case results from the combination of a normal precipitation distribution, which by definition is symmetric and has zero skew, and the linear PPT-ANPP response, which has zero curvature and preserves the zero skew in the derived ANPP distribution.

Negative (positive) curvature in the PPT-ANPP curve increases the probability of negative (positive) asymmetry in ANPP (Figure 2b, c). For a normal annual precipitation distribution, concave PPT-ANPP curves skew $f_{AI}(AI)$ toward negative values, whereas convex PPT-ANPP curves skew $f_{AI}(AI)$ toward positive values as expected. This skew is stronger for larger curvature. Using the nonlinear convex model as an example (Figure 2c), the probability of positive asymmetry increases with the exponent β which scales directly with the PPT-ANPP curve curvature, i.e., $g''(p_a) \propto \beta(\beta - 1)\omega$.

Positive skew in $f_{p_a}(p_a)$ leads to a higher probability of observing positive asymmetry in ANPP. For example, when $f_{p_a}(p_a)$ is lognormal and the PPT-ANPP curve is linear, $f_{AI}(AI)$ is positively skewed (Figure 2d) and the probability of observing $AI > 0$ is more than 50%, even though the ecosystem response is linear. Negative curvature in the PPT-ANPP curve can overcompensate for the effect of positively skewed precipitation (Figure 2e). In contrast,

This article is protected by copyright. All rights reserved.

positive curvature in the PPT-ANPP curve can amplify the effect of positively skewed precipitation (Figure 2f).

Mean annual precipitation controls the variance and skewness of AI. Lower mean annual precipitation is associated with higher variance (Fatichi et al., 2012) (Figure 2a) and higher skewness (Figure 2d) of AI. Therefore, in drier sites there is a higher probability of observing an AI far from the modal value, $AI = 0$. Further, drier sites show larger precipitation skewness and, therefore, a higher probability of observing positive asymmetry, $AI > 0$.

The length of the experiment, N, also controls the variance and skewness of AI. For ecosystems with negatively skewed AI due to a concave PPT-ANPP curve, longer experiments increase the probability of observing negative asymmetry (Figure 2b, e). Similarly, ecosystems with positively skewed AI due to a convex PPT-ANPP curve are more likely to present positive asymmetry in longer experiments (data not shown). For ecosystems with a symmetric AI distribution with equal probability of positive or negative asymmetry, longer experiments reduce the variance of AI, increasing the probability of observing a small deviation from $AI = 0$ (data not shown). From a statistical perspective, increasing N will provide a better characterization of the underlying AI population. Therefore, the sensitivity of the variance and skewness to N revealed in these model experiments indicates that undersampled systems result in either positive (e.g., linear model) or negative (e.g., concave model) bias in the AI statistics.

In summary, the asymmetry index, AI, observed in a multi-year ANPP experiment is itself a random variable and its distribution, $f_{AI}(AI)$, depends on the skewness of the annual precipitation distribution, $f_{p_a}(p_a)$, the curvature of the PPT-ANPP curve, $g(p_a)$, the length of the experiment, N, and the mean annual precipitation.

3.2 Internal and external sources of asymmetry across multiple experiments

A wide range of internal-external asymmetry combinations were identified in the 46 experiments analyzed (Figure 3a). As expected, sites with best fit normal precipitation and linear PPT-ANPP response show no asymmetry. Sites with best fit lognormal precipitation and linear PPT-ANPP response exhibit only external asymmetry. Sites with best fit normal precipitation and nonlinear PPT-ANPP response exhibit only internal asymmetry. Interestingly, sites with best fit lognormal precipitation and nonlinear PPT-ANPP response

This article is protected by copyright. All rights reserved.

show a wide range of total asymmetries. Therefore, a concave PPT-ANPP curve can either cancel or overcompensate for positive precipitation skew. Further, for lognormal precipitation and nonlinear PPT-ANPP curves, the separate internal and external asymmetries do not add to the total asymmetry (Figure 3b). This result demonstrates interactions between the precipitation skewness and ecosystem response nonlinearity in determining the mode of the *AI* distribution, although the effect is minor.

The distribution of *AI* also varies substantially across the experiments (Figure 4a). For sites with best fit normal precipitation and linear PPT-ANPP response, there is an equal probability of observing positive or negative asymmetry. Andales et al. (2006) provides an example where the best fit models were normal precipitation and linear PPT-ANPP response, yet the empirical value of *AI* was positive (Figure 4b). Most sites with best fit lognormal precipitation and linear PPT-ANPP response, have a higher probability of observing a positive asymmetry index. For some of these sites, the 95% confidence interval of the *AI* distribution did not overlap the value $AI = 0$. This indicates a strong likelihood of observing positive asymmetry in some systems with linear ecosystem responses. The Smoliak (1986) dataset provides a clear example (Figure 4c). In these cases, interpretation of positive *AI* as indicative of a nonlinear ecosystem response would be incorrect using current methods. The results for nonlinear PPT-ANPP response curves were mixed. Overall, there was a higher probability of observing negative asymmetry at these sites. For sites with skewed precipitation distributions, this implies that the PPT-ANPP response overcompensates the positive asymmetry induced by precipitation (for example, Figures 4d and 4e). Empirical *AI* values in these cases may be less negative than would be expected for symmetric precipitation distributions. Most of the calculated 95% confidence intervals overlapped the value $AI = 0$, indicating the potential for ambiguous experimental results.

The modeled asymmetry index was related to characteristics of the experiments, including precipitation mean, precipitation skewness, and experiment length (Figure 5). Notably, for experiments with lognormal precipitation and a linear PPT-ANPP response curve (i.e., all asymmetry is external), the mode of the modeled *AI* distribution decreased with mean precipitation (Figure 5g), increased with precipitation skewness (Figure 5h), and increased with experiment length (Figure 5i). That is, *AI* is more positive in drier sites with more skewed precipitation. For experiments with lognormal precipitation and concave down PPT-ANPP

This article is protected by copyright. All rights reserved.

response curve, the external *AI* increased with precipitation skewness, as expected, while the total *AI* was always negative and decreased with skewness (Figure 5e,h). The nonlinearity in the PPT-ANPP response curves overcompensated for the skewness introduced by precipitation. For all experiments, the mode of the modeled *AI* distribution became more positive or more negative as experiment length increased (Figure 5i). Consistent with the example *AI* distributions in Figure 1, there is a greater probability of estimating the true sign of total asymmetry for longer experiments.

3.3 Case Study: Konza Prairie

To isolate and demonstrate the effects of annual precipitation skewness and the curvature of the PPT-ANPP response, the linear and nonlinear concave statistical models, as well as the ecohydrological model, were applied to the Konza Prairie long-term ecological research experiment data.

3.3.1 Statistical models

Under ambient precipitation conditions at Konza Prairie, precipitation is lognormally distributed and ANPP was well approximated by a linear PPT-ANPP curve, $a = 0.43p_a + 144.1$ (Hsu et al., 2012; Knapp et al., 2017). Indeed, consistent with the model results shown in Figure 6, this dataset exhibits positive asymmetry with $AI = 0.11$. The model presented here estimated a probability of observing positive asymmetry of $P(AI > 0) = 0.75$ for this system. That is, there was a 75% probability of observing positive asymmetry considering skewness in the annual precipitation distribution alone.

When the precipitation manipulation experiment data were included, ANPP was well approximated by a nonlinear concave PPT-ANPP curve, $a = 866.3 - 298620p_a^{-1}$. Again, consistent with the model results shown in Figure 6, this dataset exhibits negative asymmetry with $AI = -0.07$. The modeled probability of observing negative asymmetry is $P(AI < 0) = 0.81$. That is, when positively skewed precipitation and concave PPT-ANPP curve are combined in this ecosystem, the model estimated an 81% probability of observing negative asymmetry. For both cases, the observed asymmetry was nearly identical to the mode of the modeled *AI* distribution (Figure 7).

This article is protected by copyright. All rights reserved.

3.3.2 Ecohydrological model

Equation (7) relates the PPT-ANPP curve to a few fundamental properties of the soil-plant-climate system. The non-linearity of this model PPT-ANPP curve is apparent on the right-hand side of equation (7), which combines gamma functions with arguments incorporating the assimilation stress point, x^*, average storm inter-arrival time, λ, and the average storm depth, α, where the annual precipitation is $p_a = \alpha\lambda T_{seas}$. PPT-ANPP curves predicted from equation (7) are illustrated in Figure 5 with data collected in the rainfall manipulation experiment at Konza Prairie (see Figure 3 in Knapp et al. (2017)). The PPT-ANPP curve shape is primarily controlled by the ratio of soil water holding capacity to the mean rainfall depth, $\gamma = nz_r(s_1 - s_w)/\alpha$. The model matches the observations for low values of $1.5 < \gamma < 5$ with the minimum root mean square error (RMSE) obtained for $\gamma = 2.8$. A value of $\gamma = 2.76$ that matches the RMSE value was estimated independently from other literature sources (see Table 1).

The results in Figure 8 demonstrate that negative curvature in the PPT-ANPP curve is a fundamental property of this model system, apparent across a wide range of parameters. Negative curvature in this model arises from two physical assumptions. First, *ET* and *A* decrease linearly with soil moisture. This drives ANPP to zero as precipitation decreases to zero. Second, the root zone water holding capacity is finite, whereas storm depths follow an exponential distribution with a finite probability of exceeding this capacity. Therefore, there is a value of annual precipitation beyond which a substantial fraction of water is lost to surface runoff or groundwater recharge and cannot be used by plants to support ANPP. Therefore, ANPP saturates at high values of annual precipitation. As γ varies the PPT-ANPP curve transitions from linear to non-linear in shape, where clear regions of zero and maximum annual productivity emerge. At both very small or large values of γ, linear regions of the curve emerge, which could confound experimental results if this region overlaps typical precipitation variability.

The sensitivity of the asymmetry index, *AI*, to climate and ecosystem properties is revealed by equation (7), which combines the soil water balance, productivity response to soil moisture, and inter-annual rainfall variability (Figure 9). The model indicates a non-linear dependence of *AI* on the rainfall skewness and the ratio of the soil water holding capacity to mean rainfall depth, γ. Positive asymmetry, $AI > 0$, is typical for low γ and high rainfall skewness. On the

This article is protected by copyright. All rights reserved.

other hand, negative asymmetry, $AI < 0$, is typical for high γ and low rainfall skewness. Therefore, ecosystems that exhibit negative asymmetry are more likely to have a higher soil water holding capacity than ecosystems that exhibit positive asymmetry.

For cases where net assimilation reaches zero before evapotranspiration, i.e., $x_{cr} > 0$, a region of positive curvature in the PPT-ANPP curve is predicted by the model for low values of annual precipitation (Figure 10a, equation S28). This PPT-ANPP curve exhibits both positive curvature, at low precipitation, and negative curvature, at high precipitation. The impact of this shape on the asymmetry index depends on the form of the annual precipitation distribution (i.e., normal or lognormal) and the mean annual precipitation. To isolate the effect of positive curvature in the PPT-ANPP curve, consider several cases with normally distributed precipitation. When the mean precipitation is near the inflection point of the PPT-ANPP curve, there is a nonlinear relationship between the mode of the AI distribution and the parameter x_{cr} (Figure 10 `b). AI is most negative for intermediate values of x_{cr}. In contrast, when the mean precipitation is lower than the inflection point of the PPT-ANPP curve, the mode of the AI distribution increases with x_{cr} (Figure 10c). As x_{cr} increases, the most likely value of AI increases and switches from negative to positive. Therefore, there is a nonlinear interaction between the precipitation distribution and the PPT-ANPP curve that determines the skewness of $f_{AI}(AI)$ and the likelihood of observing positive or negative asymmetry.

4. Discussion

Understanding the mechanisms through which climate variability drives ecosystem responses is a critical step toward assessment of climate-ecosystem interactions. Quantifying the asymmetric response of plant productivity to annual rainfall, particularly in grassland ecosystems, can have crucial implications for predictions of future global carbon cycle dynamics under varying precipitation regimes. Our results demonstrate that AI, commonly used to quantify such asymmetry, is dependent on both precipitation statistics as well as inherent ecosystem dynamics, potentially masking the true effects of precipitation on productivity. Such dependence of AI on precipitation statistics may be problematic because climate change projections suggest an increase in precipitation extremes. A change in the distribution of annual precipitation, imposed by the intensification of extremes, could strongly bias our estimates of productivity responses to rainfall under a changing climate. Specifically, our results suggest that the skewness of the annual precipitation distribution must be accounted

This article is protected by copyright. All rights reserved.

for when interpreting empirical estimates of AI. In our model, precipitation skewness in the ambient Konza Prairie experiment resulted in a 75% probability of observing positive asymmetry (Figure 7). In addition, 11 of the 46 site models resulted in positive asymmetry arising from precipitation skewness (Figure 3a). Intensification of precipitation extremes would lead to an annual precipitation distribution with a heavier tail and larger skewness. This larger skewness would likely result in an increased estimate of AI, which may not reflect a change in ecosystem dynamics, but rather a statistical artifact of the AI estimation procedure.

The AI distributions calculated using models here suggest a large uncertainty in the AI sampled during experiments (Figures 1, 4a). This uncertainty was introduced into the models entirely via the annual precipitation distribution, while the PPT-ANPP response curve shape and length of the experiment act to increase or decrease the variance and skewness derived from the precipitation distribution (Figure 2). In addition to the positive bias introduced by positively skewed precipitation, large variance in the sampled AI distribution may lead to erroneous conclusions regarding the shape of the PPT-ANPP curve. All combinations of precipitation distribution (i.e., normal or lognormal) and PPT-ANPP curve (i.e., linear, convex, concave) resulted in several sites where the 95% confidence interval of AI overlapped the value $AI = 0$ (Figure 4a). Therefore, large uncertainty in AI may confound interpretation of the ecosystem response to precipitation variability as well as cross-site comparisons.

Falsely predicting positive (concave up) ecosystem response asymmetries can be particularly detrimental as it can lead to overestimation (underestimation) of the productivity gains (losses) with climate change. Internal positive asymmetries were found to be falsely generated for several cases when precipitation skewness was high. Precipitation skewness is typically high when annual precipitation is low and, therefore, false positive asymmetries are more likely in semi-arid grasslands. Overpredicting true internal asymmetries using AI can lead to an overconservative estimation of productivity losses in semi-arid climates that are expected to become drier with climate change. This overconservative estimation might lead to overpredictions of crop yield under climate change, and potentially put a larger emphasis on the importance of semi-arid grasslands on the interannual dynamics of the global carbon cycle. Considering that the distribution of rainfall is those areas is frequently positively skewed, sampling biases are expected to play a major role (Fatichi et al., 2012).

This article is protected by copyright. All rights reserved.

On the other hand, positive precipitation skewness was often found to coincide with negative internal asymmetry (i.e., concave down ecosystem response) for low precipitation skewness in the dataset. Precipitation skewness is typically low when annual precipitation is large, common in mesic grasslands, which are not expected to experience significant water stress. Because of the precipitation skewness, the total *AI* values were less negative than would be implied by the true ecosystem response to precipitation. As rainfall skewness through the bias it introduces, overpredicts AI, this suggests a potential overestimation of productivity with climate change, especially considering that in most mesic grassland ecosystems, climate change projections suggest a rainfall increase (Ukkola et al., 2020). Considering that mesic grasslands might by more significantly limited by either other environmental factors (e.g. temperature) or nutrient limitations (Du et al., 2020; Konings et al., 2017), using *AI* as a prognostic tool could lead to false overprediction of productivity. However, precipitation skewness in those biomes is small, so the bias introduced by sampling is expected to be low (Fatichi et al., 2012).

Robust assessments of the carbon cycle response to precipitation change will require substantial effort to improve precipitation and ecosystem productivity data availability. The empirically derived AI depends on the length of the experiment N, such that longer experiments lead to improved estimates of AI (Figure 2). The experiment length is critical to properly identify non-linear ecosystem responses, particularly for rainfall manipulation experiments. Furthermore, higher order statistical properties of the precipitation distribution have been so far difficult to quantify. Positive skewness in annual precipitation distributions is common and increases with the coefficient of variation, C_v, (Fatichi et al., 2012), which is in fact a property of the lognormal distribution used here, i.e., $s \propto C_v^3$. The largest C_v was observed in semi-arid climates (Fatichi et al., 2012), which are also the strongest contributors to the interannual variability of the carbon cycle (Ahlström et al., 2015). However, quantification of skewness change is limited by the length of available data records (Fatichi et al., 2012), especially in data-poor semi-arid regions. Therefore, the sampling artifacts of AI elucidated here may strongly influence global scale carbon cycle assessment.

The asymmetry index has yielded important insights into the non-linearity of ANPP response to changing precipitation regimes (Knapp et al., 2017). However, new asymmetry metrics are needed to improve interpretation and attribution of experimental observations. For example, these approaches may include data transformations to remove precipitation skewness, non-

This article is protected by copyright. All rights reserved.

parametric statistical methods, or stochastic-dynamic system models. Asymmetry indices based on annual data, if built and assessed properly can provide important information concerning the response of annual productivity to precipitation. However, these responses, especially in semi-arid grasslands, might be highly influenced by the shorter temporal scale features of precipitation. Heisler-White et al. (2009) showed that the precipitation structure, and in particular its pulse dynamics, highly influences annual productivity. Global scale support of such an argument can also be found in recent studies that showed that annual productivity is highly dependent on a small number of hours/days when ecosystems are most active (Fatichi & Ivanov, 2014; Zscheischler et al., 2016). For this reason, detailed fine-scale ecohydrological models, driven by stochastic weather generators that inherently account for stochastic precipitation variability, can provide essential information needed to interpret empirical data.

5. Conclusion

Symmetric, asymmetric, or double asymmetric models for grassland productivity responses to annual rainfall are extremely useful prognostic tools for the responses of one of the most important biomes for global food security and global carbon management under a changing climate. Given the lack of long-term data (Knapp et al., 2017) to fit PPT-ANPP curves to observations with confidence, the AI has been extensively used to diagnose such asymmetries. However, our results show that AI can be heavily biased by the sampling distribution of annual rainfall and the sample size, leading to incorrect assessments of true nonlinear ecosystem response to climatic forcing (i.e., “internal” ecosystem asymmetry). It is reasonable to expect other ecosystem variables and metrics influenced by skewed climate drivers may suffer from similar biases.

Acknowledgments

A. Parolari acknowledges support from a summer faculty fellowship from Marquette University and A. Paschalis acknowledges support from NERC (grant no. NE/S003495/1). The authors thank Michael Goulden and Alan Knapp for comments on an early version of this manuscript.

Author contributions

A.J.P. designed the research and developed the models; A.J.P. and A.P. analyzed the data, interpreted the results, and wrote the manuscript.

This article is protected by copyright. All rights reserved.

Data availability statement

Code and data used for model simulations and to produce figures available from the Dryad Digital Repository: <https://doi.org/10.5061/dryad.r7sqv9scz> (Parolari et al. 2021).

References

Abramowitz, M., & Stegun, I. A. (1972). Handbook of mathematical functions with formulas, grpahs and mathematical tables. *National Bureau of Standards - Applied Mathematics Series*. https://doi.org/10.1119/1.15378

Ahlström, A., Raupach, M. R., Schurgers, G., Smith, B., Arneth, A., Jung, M., et al. (2015). The dominant role of semi-arid ecosystems in the trend and variability of the land CO2 sink. *Science*, *348*(6237), 895–899. https://doi.org/10.1126/science.aaa1668

Andales, A. A., Derner, J. D., Ahuja, L. R., & Hart, R. H. (2006). Strategic and tactical prediction of forage production in northern mixed-grass prairie. *Rangeland Ecology and Management*, *59*(6). https://doi.org/10.2111/06-001R1.1

Bai, Y., Han, X., Wu, J., Chen, Z., & Li, L. (2004). Ecosystem stability and compensatory effects in the Inner Mongolia grassland. *Nature*, *431*(7005). https://doi.org/10.1038/nature02850

Bai, Y. F., Li, L. H., Huang, J. H., & Chen, Z. Z. (2001). The influence of plant diversity and functional composition on ecosystem stability of four Stipa communities in the inner Mongolia Plateau. *Acta Botanica Sinica*, *43*(3).

Daly, E., Porporato, A., & Rodriguez-Iturbe, I. (2004). Coupled Dynamics of Photosynthesis, Transpiration, and Soil Water Balance. Part II: Stochastic Analysis and Ecohydrological Significance. *Journal of Hydrometeorology*, *5*(3), 559–566. https://doi.org/10.1175/1525-7541(2004)005<0559:cdopta>2.0.co;2

Du, E., Terrer, C., Pellegrini, A. F. A., Ahlström, A., van Lissa, C. J., Zhao, X., et al. (2020). Global patterns of terrestrial nitrogen and phosphorus limitation. *Nature Geoscience*, *13*(3). https://doi.org/10.1038/s41561-019-0530-4

Easterling, D. R. (2000). Climate Extremes: Observations, Modeling, and Impacts. *Science*, *289*(5487), 2068–2074. https://doi.org/10.1126/science.289.5487.2068

Fatichi, S., & Ivanov, V. Y. (2014). Interannual variability of evapotranspiration and vegetation productivity. *Water Resources Research*, *50*(4), 3275–3294. https://doi.org/10.1002/2013WR015044

Fatichi, S., Ivanov, V. Y., & Caporali, E. (2012). Investigating interannual variability of precipitation at the global scale: Is there a connection with seasonality? *Journal of Climate*, *25*(16), 5512–5523. https://doi.org/10.1175/JCLI-D-11-00356.1

Fay, P. A., Carlisle, J. D., Knapp, A. K., Blair, J. M., & Collins, S. L. (2000). Altering rainfall timing and quantity in a mesic grassland ecosystem: Design and performance of rainfall manipulation shelters. *Ecosystems*, *3*(3), 308–319. https://doi.org/10.1007/s100210000028

Feng, X., Vico, G., & Porporato, A. (2012). On the effects of seasonality on soil water balance and plant growth. *Water Resources Research*, *48*(5), 1–12. https://doi.org/10.1029/2011WR011263

Fischer, E. M., & Knutti, R. (2015). Anthropogenic contribution to global occurrence of heavy-precipitation and high-temperature extremes. *Nature Climate Change*, *5*(6), 560–564. https://doi.org/10.1038/nclimate2617

Greve, P., & Seneviratne, S. I. (2015). Assessment of future changes in water availability and aridity. *Geophysical Research Letters*, *42*(13). https://doi.org/10.1002/2015GL064127

This article is protected by copyright. All rights reserved.

Haverd, V., Ahlström, A., Smith, B., & Canadell, J. G. (2017). Carbon cycle responses of semi-arid ecosystems to positive asymmetry in rainfall. *Global Change Biology*, *23*(2), 793–800. https://doi.org/10.1111/gcb.13412

Heisler-White, J. L., Blair, J. M., Kelly, E. F., Harmoney, K., & Knapp, A. K. (2009). Contingent productivity responses to more extreme rainfall regimes across a grassland biome. *Global Change Biology*, *15*(12), 2894–2904. https://doi.org/10.1111/j.1365-2486.2009.01961.x

Hoover, D. L., Knapp, A. K., & Smith, M. D. (2014). Resistance and resilience of a grassland ecosystem to climate extremes. *Ecology*, *95*(9), 2646–2656. https://doi.org/10.1890/13-2186.1

Hsu, J. S., Powell, J., & Adler, P. B. (2012). Sensitivity of mean annual primary production to precipitation. *Global Change Biology*, *18*(7), 2246–2255. https://doi.org/10.1111/j.1365-2486.2012.02687.x

Humphrey, V., Zscheischler, J., Ciais, P., Gudmundsson, L., Sitch, S., & Seneviratne, S. I. (2018). Sensitivity of atmospheric CO2 growth rate to observed changes in terrestrial water storage. *Nature*, *560*(7720), 628–631. https://doi.org/10.1038/s41586-018-0424-4

Istanbulluoglu, E., Wang, T., & Wedin, D. A. (2012). Evaluation of ecohydrologic model parsimony at local and regional scales in a semiarid grassland ecosystem. *Ecohydrology*, *5*(March), 121–142. https://doi.org/10.1002/eco.211

Knapp, A. K., & Smith, M. D. (2001). Variation Among Biomes in Temporal Dynamics of Aboveground Primary Production. *Science*, *291*(5503), 481–484. https://doi.org/10.1126/science.291.5503.481

Knapp, A. K., Harper, C. W., Danner, B. T., & Lett, M. S. (2002). Rainfall Variability , Carbon Cycling , and Plant Species Diversity in a Mesic Grassland. *Science*, *298*(298), 2202–2206. https://doi.org/10.1126/science.1076347

Knapp, A. K., Beier, C., Briske, D. D., Classen, A. T., Luo, Y., Reichstein, M., et al. (2008). Consequences of More Extreme Precipitation Regimes for Terrestrial Ecosystems. *BioScience*, *58*(9), 811–821. https://doi.org/10.1641/B580908

Knapp, A. K., Ciais, P., & Smith, M. D. (2017). Reconciling inconsistencies in precipitation–productivity relationships: implications for climate change. *New Phytologist*, *214*(1), 41–47. https://doi.org/10.1111/nph.14381

Konings, A. G., Williams, A. P., & Gentine, P. (2017). Sensitivity of grassland productivity to aridity controlled by stomatal and xylem regulation. *Nature Geoscience*, *10*(4). https://doi.org/10.1038/ngeo2903

Koutroulis, A. G. (2019). Dryland changes under different levels of global warming. *Science of the Total Environment*, *655*. https://doi.org/10.1016/j.scitotenv.2018.11.215

Kunkel, K. E., Karl, T. R., Brooks, H., Kossin, J., Lawrimore, J. H., Arndt, D., et al. (2013). Monitoring and understanding trends in extreme storms: State of knowledge. *Bulletin of the American Meteorological Society*, *94*(4), 499–514. https://doi.org/10.1175/BAMS-D-11-00262.1

Lenderink, G., & Van Meijgaard, E. (2008). Increase in hourly precipitation extremes beyond expectations from temperature changes. *Nature Geoscience*, *1*(8), 511–514. https://doi.org/10.1038/ngeo262

Molnar, P., Fatichi, S., Gaál, L., Szolgay, J., & Burlando, P. (2015). Storm type effects on super Clausius-Clapeyron scaling of intense rainstorm properties with air temperature. *Hydrology and Earth System Sciences*, *19*(4). https://doi.org/10.5194/hess-19-1753-2015

Moustakis, Y., Onof, C. J., & Paschalis, A. (2020). Atmospheric convection, dynamics and topography shape the scaling pattern of hourly rainfall extremes with temperature globally. *Communications Earth & Environment*. https://doi.org/10.1038/s43247-020-0003-0

This article is protected by copyright. All rights reserved.

Moustakis, Y., Papalexiou, S. M., Onof, C. J., & Paschalis, A. (2021). Seasonality, Intensity, and Duration of Rainfall Extremes Change in a Warmer Climate. *Earth's Future*. https://doi.org/10.1029/2020EF001824

O'Mara, F. P. (2012). The role of grasslands in food security and climate change. *Annals of Botany*. https://doi.org/10.1093/aob/mcs209

Parolari, A. J., Goulden, M. L., & Bras, R. L. (2015). Ecohydrological controls on grass and shrub above-ground net primary productivity in a seasonally dry climate. *Ecohydrology*, *8*(8), 1572–1583. https://doi.org/10.1002/eco.1605

Pendergrass, A. G., & Knutti, R. (2018). The Uneven Nature of Daily Precipitation and Its Change. *Geophysical Research Letters*, *45*(21), 11980–11988. https://doi.org/10.1029/2018GL080298

Peterson, T. C., Heim, R. R., Hirsch, R., Kaiser, D. P., Brooks, H., Diffenbaugh, N. S., et al. (2013). Monitoring and understanding changes in heat waves, cold waves, floods, and droughts in the United States: State of knowledge. *Bulletin of the American Meteorological Society*, *94*(6), 821–834. https://doi.org/10.1175/BAMS-D-12-00066.1

Piao, S., Wang, X., Wang, K., Li, X., Bastos, A., Canadell, J. G., et al. (2020). Interannual variation of terrestrial carbon cycle: Issues and perspectives. *Global Change Biology*. https://doi.org/10.1111/gcb.14884

Porporato, A., Daly, E., & Rodriguez-Iturbe, I. (2004). Soil water balance and ecosystem response to climate change. *American Naturalist*, *164*(5), 625–632. https://doi.org/10.1086/424970

Porporato, A., Vico, G., & Fay, P. A. (2006). Superstatistics of hydro-climatic fluctuations and interannual ecosystem productivity. *Geophysical Research Letters*, *33*(15). https://doi.org/10.1029/2006GL026412

Poulter, B., Frank, D., Ciais, P., Myneni, R. B., Andela, N., Bi, J., et al. (2014). Contribution of semi-arid ecosystems to interannual variability of the global carbon cycle. *Nature*, *509*(7502), 600–603. https://doi.org/10.1038/nature13376

Smoliak, S. (1986). Influence of Climatic Conditions on Production of Stipa-Bouteloua Prairie over a 50-Year Period. *Journal of Range Management*, *39*(2). https://doi.org/10.2307/3899276

Ukkola, A. M., de Kauwe, M. G., Roderick, M. L., Abramowitz, G., & Pitman, A. J. (2020). Robust Future Changes in Meteorological Drought in CMIP6 Projections Despite Uncertainty in Precipitation. *Geophysical Research Letters*, *47*(11). https://doi.org/10.1029/2020GL087820

Wilcox, K. R., Blair, J. M., Smith, M. D., & Knapp, A. K. (2016). Does ecosystem sensitivity to precipitation at the site-level conform to regional-scale predictions? *Ecology*, *97*(3), 561–568. https://doi.org/10.1890/15-1437

Wu, D., Ciais, P., Viovy, N., Knapp, A. K., Wilcox, K., Bahn, M., et al. (2018). Asymmetric responses of primary productivity to altered precipitation simulated by ecosystem models across three long-term grassland sites. *Biogeosciences*, *15*(11), 3421–3437. https://doi.org/10.5194/bg-15-3421-2018

Zscheischler, J., Fatichi, S., Wolf, S., Blanken, P. D., Bohrer, G., Clark, K., et al. (2016). Short-term favorable weather conditions are an important control of interannual variability in carbon and water fluxes. *Journal of Geophysical Research: Biogeosciences*, *121*(8), 2186–2198. https://doi.org/10.1002/2016JG003503

This article is protected by copyright. All rights reserved.

Table 1. Model parameters estimated from previous studies at Konza Prairie (Heisler-White et al., 2009; Knapp et al., 2017; Porporato et al., 2004, 2006)

Parameter		Units	Value
Root depth	z_r	mm	300
Porosity	n	-	0.52
Field capacity	s_1	-	0.67
Wilting point	s_w	-	0.34
Mean rainfall depth	α	mm	11.4
Maximum potential evapotranspiration	ET_{max}	mm d^{-1}	4.5
Maximum daily net assimilation	A_{max}	g DM m^{-2} d^{-1}	3.8
Assimilation stress point	s^*	-	0.6
Growing season length	T_{seas}	d	183

Accepted Article

This article is protected by copyright. All rights reserved.

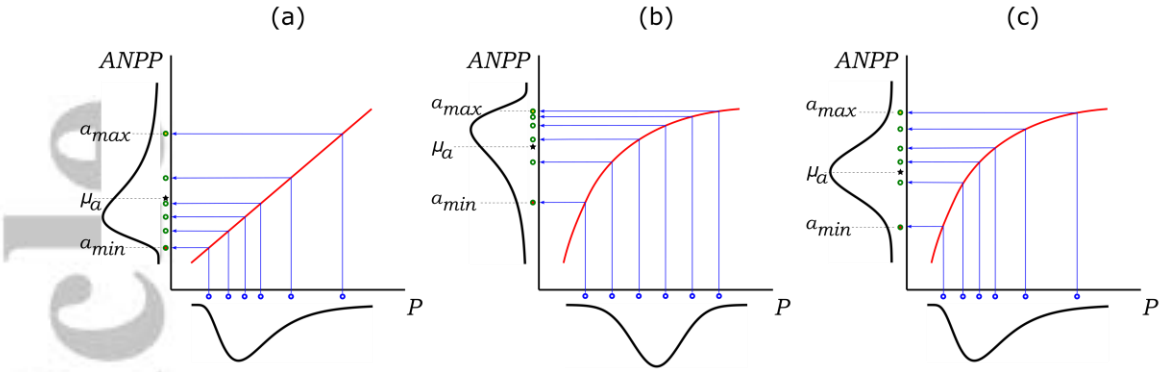


Figure 1. Examples of the annual precipitation distribution influence on estimated asymmetry index (*AI*) in ANPP experiments. (a) When the precipitation distribution is positive skewed and the PPT-ANPP response curve is linear, ANPP experiments will yield a positive *AI*, leading to an incorrect conclusion regarding the nonlinearity of the ANPP response to precipitation. (b) When the precipitation distribution is symmetric (e.g., normal) and the PPT-ANPP response curve is nonlinear concave, positive ANPP deviations are smaller than negative deviations and *AI* is correctly estimated as negative. (c) When the precipitation distribution is positive skewed and the PPT-ANPP response curve is concave, the ecosystem response can offset some or all of the positive asymmetry introduced by the precipitation statistics, confounding the relationship between experimentally determined *AI* and the nonlinearity of the ANPP response to precipitation.

Accepted Article

This article is protected by copyright. All rights reserved.

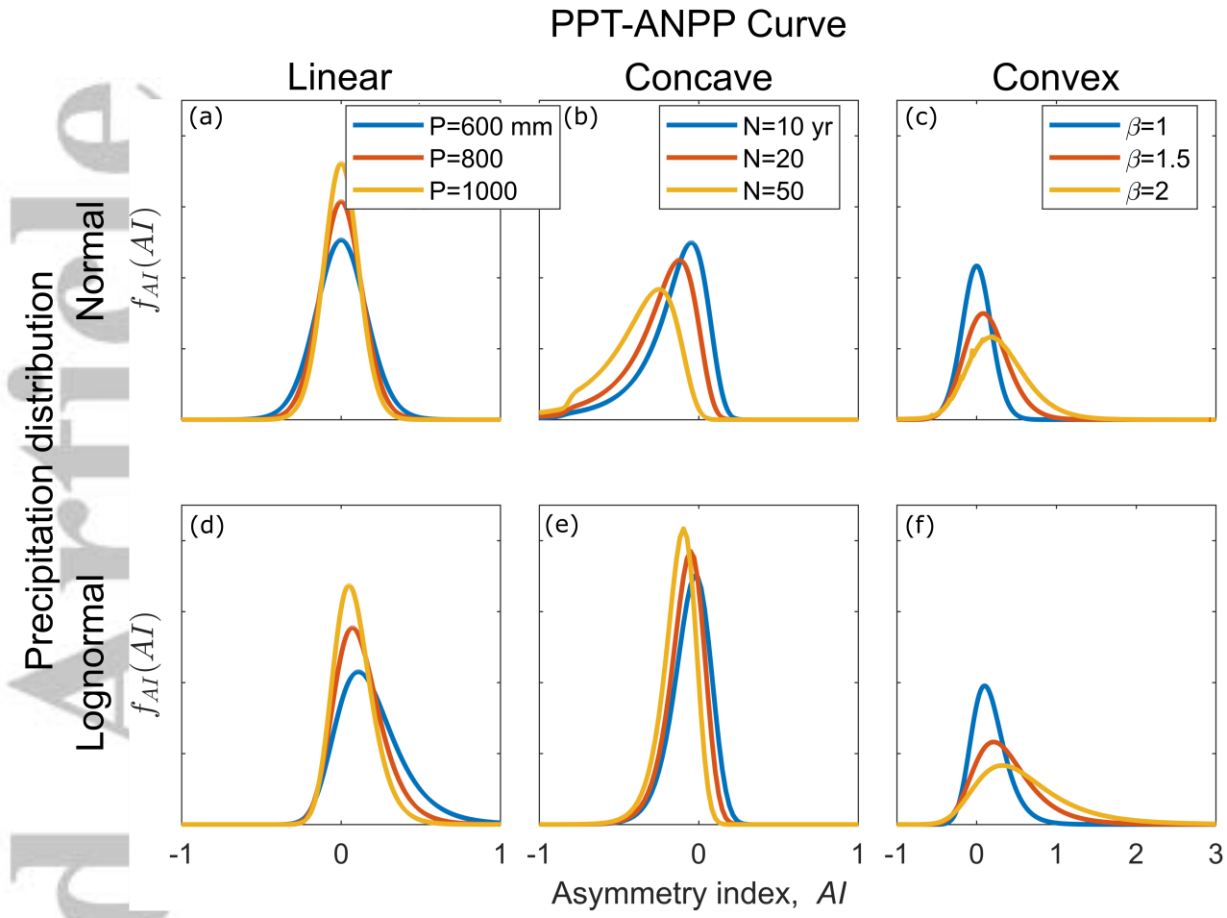


Figure 2. The probability density function (PDF) of the asymmetry index, $f_{AI}(AI)$, for different combinations of annual precipitation distribution (normal, top; lognormal, bottom) and PPT-ANPP curves (linear, left; nonlinear concave, middle; nonlinear convex, right). The influence of several parameters on the distribution of AI are also shown: the mean annual precipitation, P, the experiment length, N, and the convexity of the PPT-ANPP curve, controlled by the exponent, β.

This article is protected by copyright. All rights reserved.

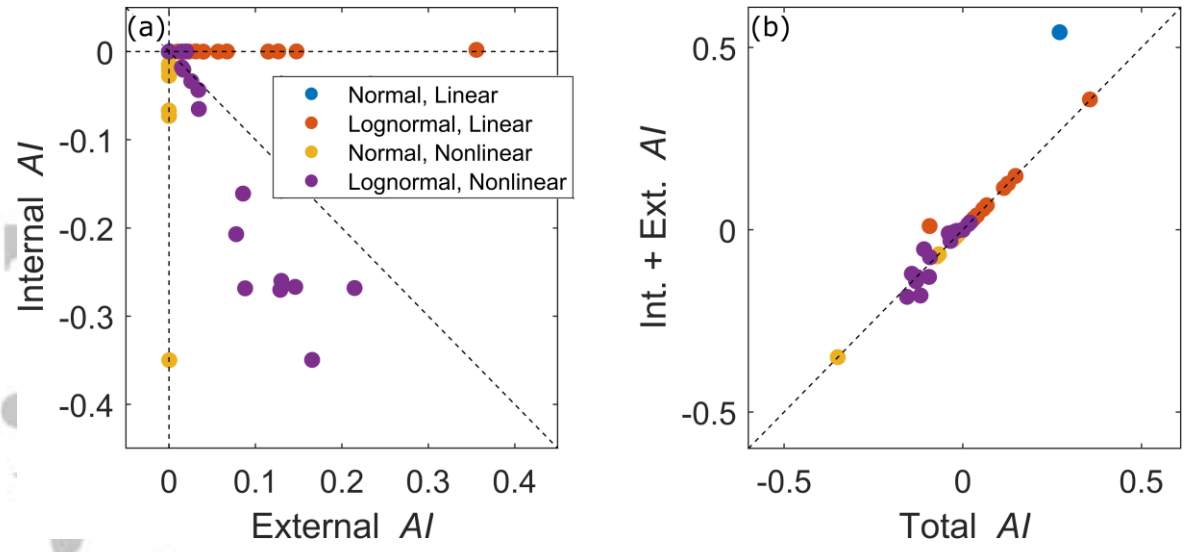


Figure 3. (a) Decomposition of modeled internal and external asymmetry indices and (b) comparison of modeled total asymmetry index to the sum of modeled internal and external asymmetry indices for the grassland experiments compiled in the Hsu et al. (2012) dataset. Colors correspond to the following precipitation distribution, PPT-ANPP curve pairs: blue (linear, normal); red (linear, lognormal); yellow (nonlinear, normal); purple (nonlinear, lognormal). In (a), the diagonal line denotes nonlinear, lognormal sites where positive precipitation skew is exactly compensated by ANPP-PPT curve saturation. Sites that fall below this line have negative total asymmetry resulting from overcompensation by ANPP-PPT curve saturation. Note there are no sites with positive total asymmetry because the PPT-ANPP curves were assumed to be either linear or nonlinear concave (equations 5 and 6).

Accepted Article

This article is protected by copyright. All rights reserved.

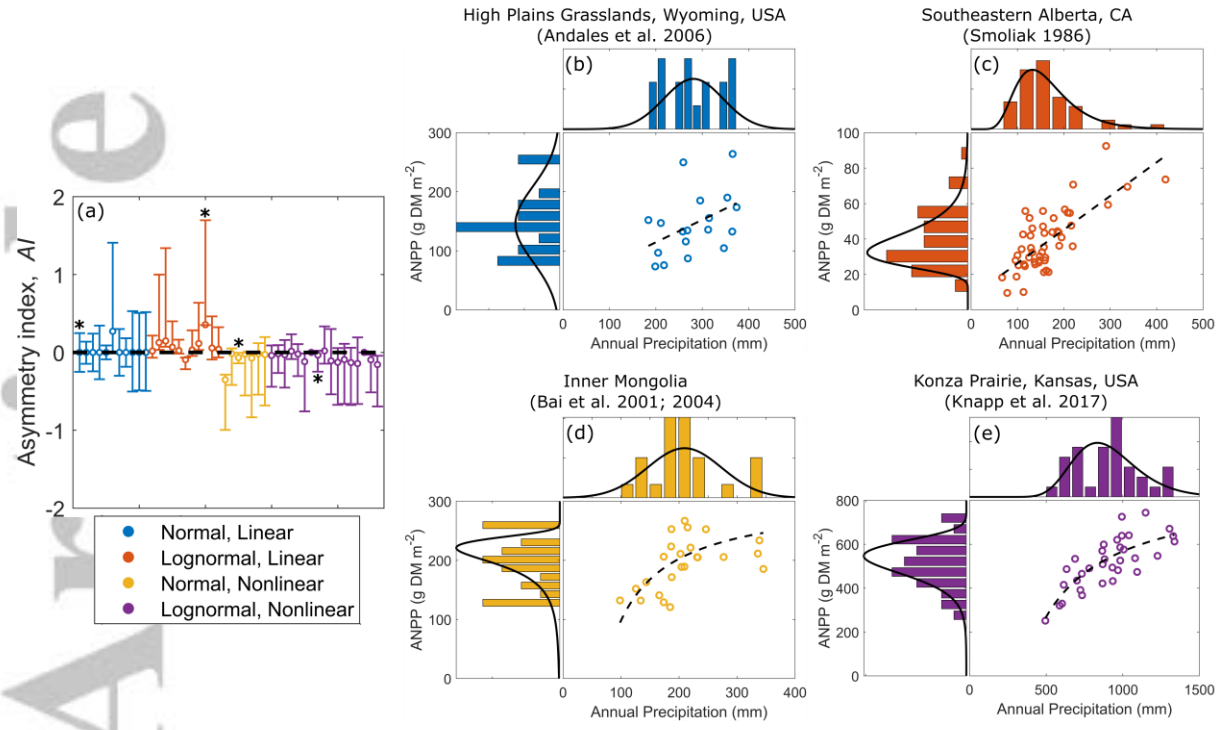


Figure 4. (a) Modes and 95% confidence intervals of the modeled asymmetry index distributions for the grassland experiments compiled in the Hsu et al. (2012) dataset. (b)-(e) Example best fit annual precipitation distributions, best fit PPT-ANPP curves, and ANPP distributions illustrating each of the 4 combinations of normal/lognormal precipitation distributions and linear/nonlinear PPT-ANPP curves (AI distributions marked by the asterisks in (a)) (Andales et al., 2006; Y. Bai et al., 2004; Y. F. Bai et al., 2001; Smoliak, 1986).

This article is protected by copyright. All rights reserved.

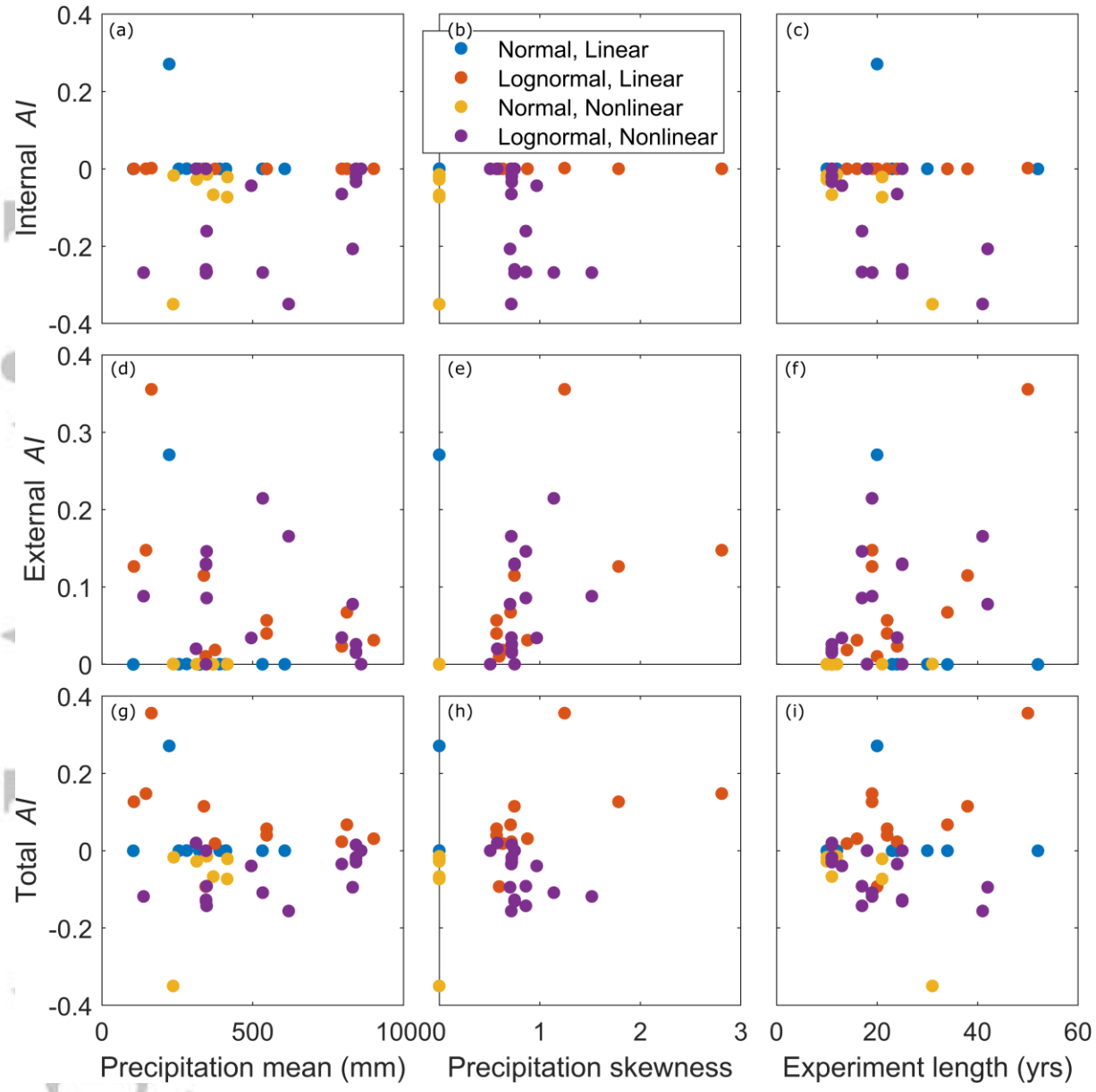


Figure 5. Mode of the modeled asymmetry index distributions as a function of (a,d,g) annual precipitation mean, (b,e,h) annual precipitation skewness, and (c,f,i) experiment length. The internal *AI* due to PPT-ANPP response (a-c), external *AI* due to precipitation skewness (d-f), and total *AI* (g-i) are shown.

This article is protected by copyright. All rights reserved.

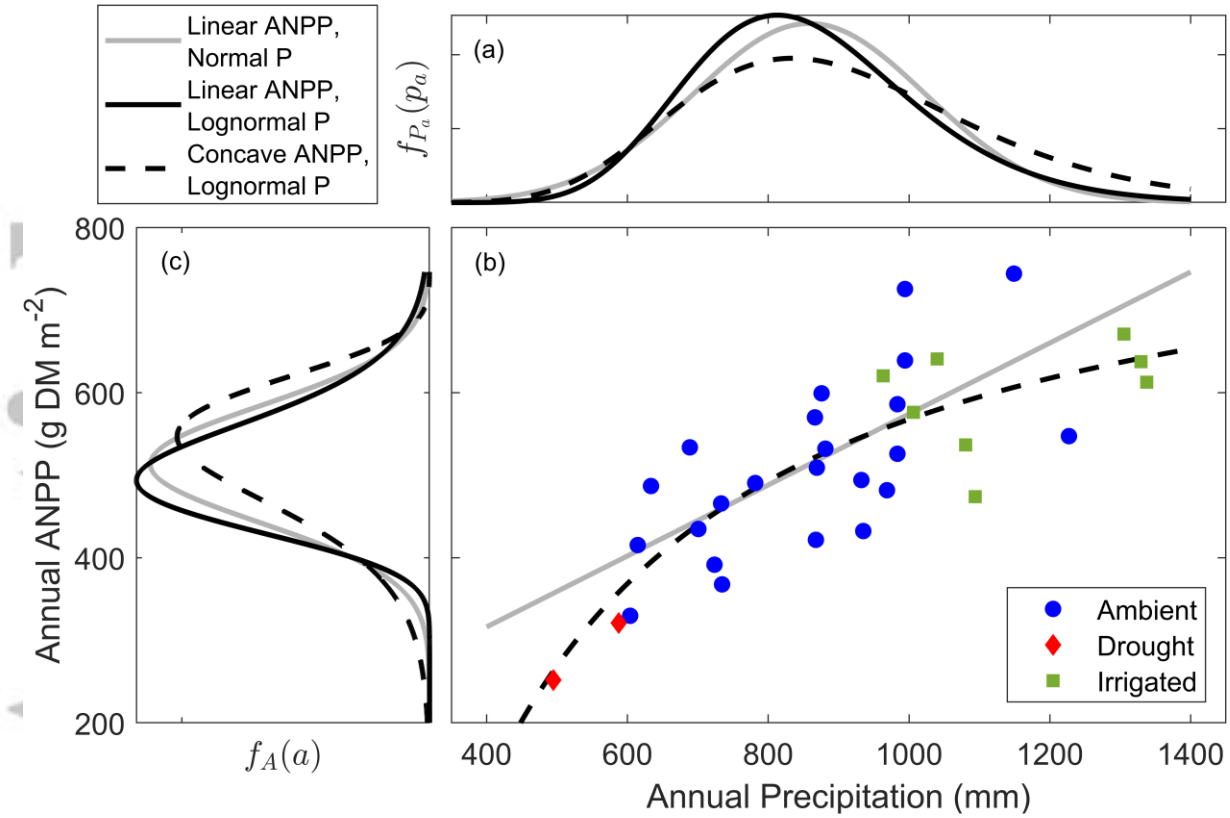


Figure 6. Separate contributions of (a) positively skewed precipitation and (b) nonlinear concave PPT-ANPP response curve to (c) asymmetry in the inter-annual ANPP distribution for the Konza Prairie long-term ANPP experiment. The linear PPT-ANPP curve with a normal precipitation distribution results in a symmetric ANPP distribution (gray curves in (a), (b), and (c)). Because the observed precipitation distribution is positively skewed, the ANPP distribution for the linear PPT-ANPP curve (fit to the ambient data, blue dots) is also positively skewed (solid black curves in (a) and (c)). For the nonlinear concave PPT-ANPP curve (fit to the ambient and precipitation manipulation data, blue, red, and green dots), the ANPP distribution is negatively skewed (dashed black curves in (a), (b), and (c)). In (b), the blue dots denote ambient precipitation, the red dots denote drought treatment, and the green dots denote irrigation treatment.

Accepted

This article is protected by copyright. All rights reserved.

Accepted Article

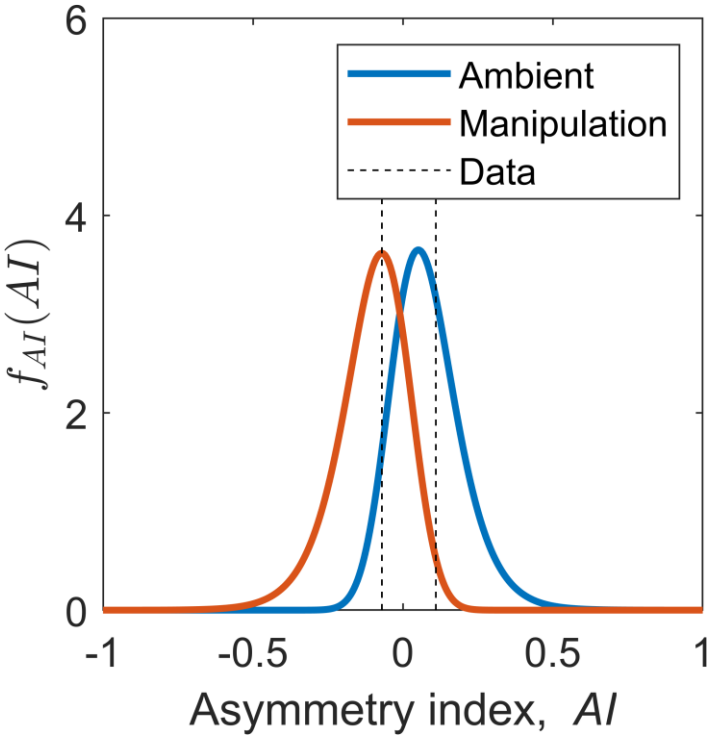


Figure 7. Modeled distribution of the asymmetry index, $f_{AI}(AI)$, for the ambient and manipulation cases at Konza Prairie. The dashed lines correspond to the values of AI calculated from the data with equation (1).

This article is protected by copyright. All rights reserved.

Accepted Article

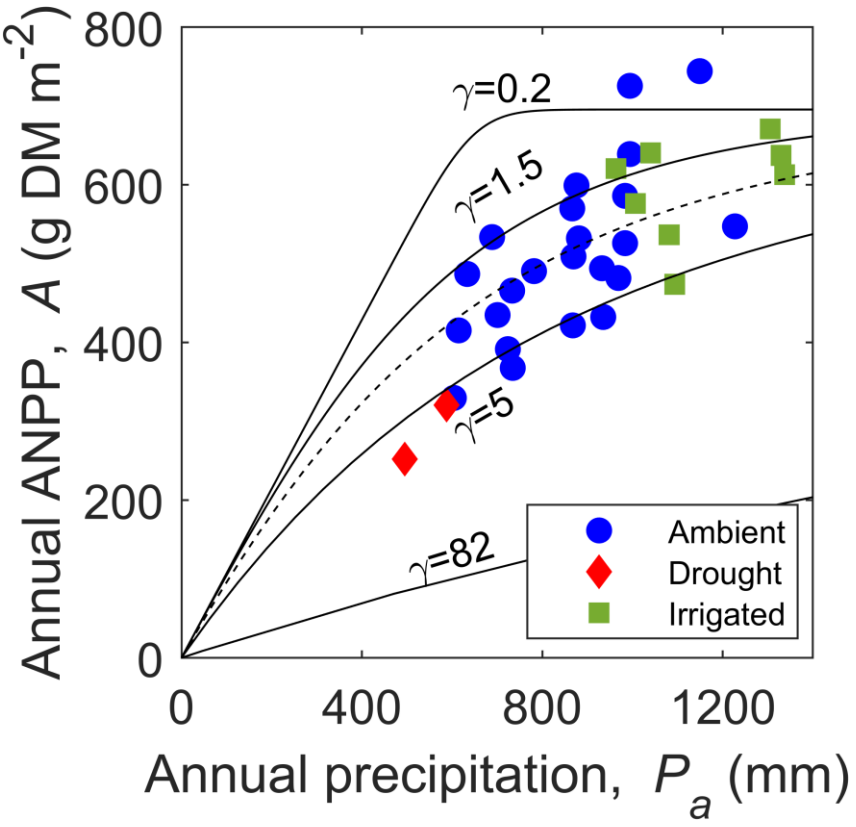


Figure 8. PPT-ANPP curves predicted by the minimalist model for non-seasonal climates (equation 7). The dashed black line corresponds to the minimum RMSE fit to the data ($\gamma = 2.8$) and the solid black lines illustrate the range $1.5 < \gamma < 5$ and limiting values of γ that produce regions of nearly linear PPT-ANPP response ($\gamma = 0.2$ and $\gamma = 82$). Parameters are given in Table 1. Annual precipitation is varied by varying λ while $\alpha = 11.4$ mm is held constant (Porporato et al., 2006). The data points are from the Konza Prairie LTER (Hoover et al., 2014; Knapp et al., 2017; Wilcox et al., 2016).

This article is protected by copyright. All rights reserved.

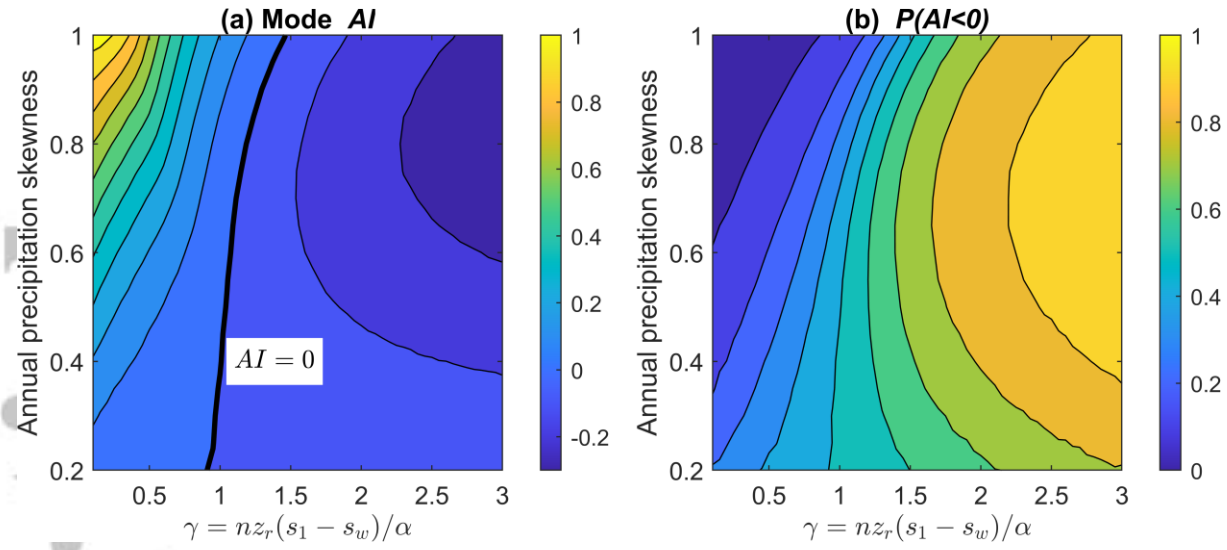


Figure 9. (a) Mode of asymmetry index (AI) and (b) the probability of observing negative asymmetry (i.e., $AI < 0$) as a function of the ratio of soil water holding capacity to mean rainfall depth, γ, and the skewness of the annual precipitation distribution, as predicted by the minimalist PPT-ANPP model (equation 7). The value of AI plotted is the mode of the underlying distribution $f_{AI}(AI)$. Mean annual rainfall is 800 mm and other parameters are given in Table 1.

Accepted Article

This article is protected by copyright. All rights reserved.

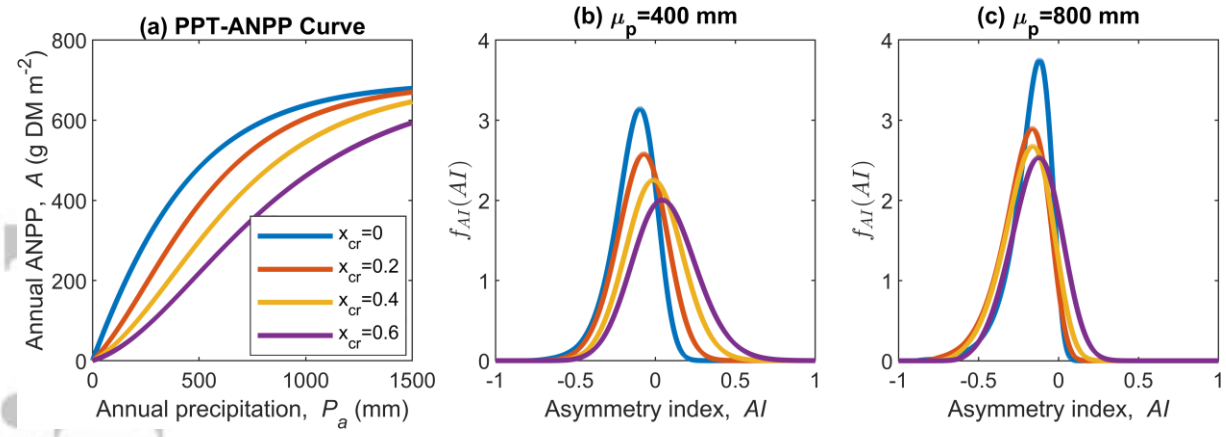


Figure 10. The effect of water-limited net assimilation on (a) the physically-based PPT-ANPP curve and the asymmetry index distribution, $f_{AI}(AI)$, for (b) mean precipitation of 800 mm and (c) mean precipitation of 400 mm. The precipitation distribution is assumed to be normal and all other parameters are given in Table 1.

Accepted Article

This article is protected by copyright. All rights reserved.